

Cost-effective On-device Continual Learning over Memory Hierarchy with Miro

Xinyue Ma
UNIST
xinyuema@unist.ac.kr

Suyeon Jeong
UNIST
suyeonj@unist.ac.kr

Minjia Zhang
Microsoft
minjiaz@microsoft.com

Di Wang
Unaffiliated
diwangbruce@gmail.com

Jonghyun Choi
Yonsei University
jc@yonsei.ac.kr

Myeongjae Jeon
UNIST
mjjeon@unist.ac.kr

ABSTRACT

Continual learning (CL) trains NN models incrementally from a continuous stream of tasks. To remember previously learned knowledge, prior studies store old samples over a memory hierarchy and replay them when new tasks arrive. Edge devices that adopt CL to preserve data privacy are typically energy-sensitive and thus require high model accuracy while not compromising energy efficiency, i.e., cost-effectiveness. Our work is the first to explore the design space of hierarchical memory replay-based CL to gain insights into achieving cost-effectiveness on edge devices. We present Miro, a novel system runtime that carefully integrates our insights into the CL framework by enabling it to dynamically configure the CL system based on resource states for the best cost-effectiveness. To reach this goal, Miro also performs online profiling on parameters with clear accuracy-energy trade-offs and adapts to optimal values with low overhead. Extensive evaluations show that Miro significantly outperforms baseline systems we build for comparison, consistently achieving higher cost-effectiveness.

1 INTRODUCTION

As the demand for realistic on-device machine learning (ML) has grown, learning paradigms well-suited for mobile and edge devices have attracted significant attention. One such paradigm is continual learning (CL), which performs model training *incrementally* as new data (e.g., new face images) becomes available. The neural network (NN) models in CL running on devices learn new knowledge from data without dependencies on scalable compute resources provided by external servers, preserving strong data privacy. As *on-device CL* research is getting mature for its system and data efficiency [27, 34, 56], we anticipate it to gain prominence in many privacy-sensitive tasks on the edge, such as user personalization [18, 21, 40], home automation [40, 61], smart healthcare [36, 53], wearable devices [47], and video analytics [11, 32, 49].

However, any CL algorithms, including the on-device CL, must overcome *catastrophic forgetting* to realize their full

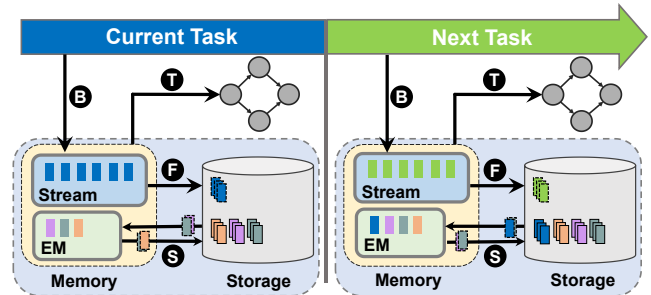


Figure 1: Architecture and execution stages of HEM.

potential [39]. CL undergoing severe forgetting will have the previously learned knowledge quickly fading away while learning new data. ML researchers have extensively explored this issue, and episodic memory (EM) has been recognized as one of the most effective approaches [13, 16, 17, 38, 42]. With the EM, CL stores old samples in the memory and *replays* them when new samples are used to train a model for preserving past knowledge. Edge devices typically have limited memory capacity (4–12 GB) for all on-device programs, making it difficult to dedicate ample memory space solely for EM although large-sized EM promises high performance. Consequently, researchers have begun exploring a pragmatic system design for EM over a deep memory Hierarchy (or HEM) [35], including small memory with fast access (50–150 ns) and large storage with slow access (25–250 μ s).

EM over Memory Hierarchy (HEM). The HEM builds upon the existing EM-based CL methods, as shown in Figure 1, while considering both system efficiency and prediction accuracy. HEM organizes EM in RAM to retrieve a small set of old samples at high speed during training. At the same time, HEM stores a large number of old samples in storage and uses them to improve model accuracy by performing *data swapping*. The data swapping is an online process that replaces the samples in the EM drawn by model training (i.e., old samples replayed to mitigate the forgetting) with other old samples in the storage. The HEM can be configured to replace a small portion of the EM samples to reduce *data*

Insight

1. GPU dominates dynamic power. Thus, perform data swapping as needed without concern for its impact on power usage.
2. Using larger memory for new and old tasks often harms cost-effectiveness. No silver-bullet solution to memory allocation exists. Thus, make informed dynamic decisions for the current CL setup.
3. The epoch count required to achieve near-highest accuracy is observed to remain consistent over consecutive training tasks. Attempts to reduce this count may have negative consequences. So, use the known good value or search it for the first few tasks.

Table 1: Key insights from our study of on-device CL.

swapping costs. With HEM, CL can constantly retrieve information from a large corpus of past data to memorize it without needing to increase model capacity.

HEM is suited to hardware requirements of edge computing systems for several reasons. (1) Removable storage devices are cheap. For example, one of our reference platforms, NVIDIA Jetson TX2, is equipped with 8 GB RAM and 32 GB eMMC flash, and its storage can be easily extended with a 256 GB microSD card at only around 20 USD. (2) Sustainable I/O traffic is low. The eMMC flash drive in Jetson TX2 serves I/O requests at around 400 MB/s (and ~ 100 MB/s for microSD); in comparison, NVMe SSDs in modern AI servers support I/O rates up to 3.5 GB/s. However, by swapping only a small number of EM samples, it is possible for HEM to match those low I/O bandwidth storage. (3) Processing capabilities of mobile GPUs are not powerful enough. HEM’s key advantage lies in enhancing the data diversity of traditional EM-based CL methods without inducing additional computational costs, which can hamper edge AI GPUs and manifest as longer training times.

Efficient and Practical HEM. Recent studies like CarM [35] have demonstrated that HEM can remarkably improve model accuracy in image classification. However, evaluating HEM has been limited to a proof of concept and overlooked the most important metric of edge devices, *energy efficiency*. Moreover, CarM conducted experiments mainly focused on a few constant swapping ratios on an AI server with hardware specifications vastly different from ordinary edge devices. These swapping ratios were neither systematically chosen nor based on the consideration of energy spending associated with EM size and data movements between storage and memory.

In this work, we take a step toward building more practical on-device continual learning by exploring the design space of HEM using various edge platforms and workloads and providing valuable insights with the real-world evaluation metric of energy consumption. Also, we showcase a new system runtime that optimizes HEM for high *cost-effectiveness*, which achieves high prediction accuracy with lower energy consumption, under diverse resource constraints of target devices.

Contributions. We make the following contributions:

- *Systematic study of on-device CL.* To the best of our knowledge, this work presents the most comprehensive exploration of on-device CL over memory hierarchy to date. We compare the performance, accuracy, and energy efficiency of various points in the design space of HEM, as listed in Table 2. Our study spans two popular NN models and two CL methods designed for Computer Vision (CV). Our study provides key insights as summarized in Table 1.

- *System runtime for HEM.* Our exploration study breaks new ground in cost-effective on-device CL. As a result, we develop Miro, a new system runtime that optimizes HEM for cost-effectiveness based on the insights we have gained from our study. A key challenge is configuring the various design parameters in Table 2 without compromising accuracy and energy efficiency. To address this challenge, we categorize these parameters into three types: *Static*, *Capacity*, and *Trade-off*, and employ different optimization techniques for each type. For example, the data swap ratio is a capacity-bound parameter with minimal impact on system-wide energy usage. Hence, Miro only controls I/O congestion and attempts to make the most of the available I/O bandwidth. In contrast, Miro dynamically determines the optimal memory space for new and old tasks while considering their accuracy-energy trade-offs, which can vary significantly over time. To make informed choices, Miro estimates accuracies and energy expenses of potential size pairs via lightweight online profiling, identifies promising configurations, and applies a cost-effectiveness metric called *utility* to select the most viable candidate. We propose several cost-reduction techniques to make profiling more manageable in practice.

Experimental Results. We build Miro atop the state-of-the-art HEM-based CL system CarM and evaluate its efficacy against baseline systems we implement for comparison on five datasets across three task domains, including image classification, audio classification, and human activity recognition, as shown in Table 3. In small to medium-scale experiments, Miro consumes 7–66% less energy while achieving 1.35–15.37% higher accuracy across various memory budgets compared to the baseline systems. In large-scale experiments with the ImageNet1k dataset, Miro achieves 46.05% energy savings and 23.37% higher accuracy compared to CarM. Due to our cost-saving efforts, our profiler is 346 \times faster than an exhaustive one that uses all epochs and samples and adds only around 7–10% overhead, which can easily be offset by the benefits that Miro delivers.

2 CONTINUAL LEARNING ON HEM

In continual learning (CL), the NN model is trained with a stream of non-IID data. This input data is typically organized as multiple tasks, where a task may include data that

diverges from past data, which is referred to as *data drift*. Examples include (1) unseen object appearances, scenes, and lighting conditions for video stream analytics [11, 32], (2) new real-life activities and gestures for human activity recognition [34], and (3) new identity of the individuals and pets for household robots [27, 61].

These scenarios often necessitate timely outcomes from training. For instance, consider anomaly detection in video stream analytics that aims to identify abnormal objects or actions in images captured by surveillance cameras, drones, or robots. In such cases, an initially deployed model cannot identify all possible abnormal events in advance. Since anomalies demand immediate attention, updating models promptly is essential: postponing training to unpredictable intervals (e.g., device charging) would limit the applicability of CL. Moreover, not all mobile and edge devices have sufficient memory to accommodate training data due to heterogeneous hardware resource constraints. The purpose of Miro is to tackle these intricate challenges and broaden the scope of scenarios in which CL can be effectively applied to.

Workflow. In edge devices, storage can be used to store and replay a large amount of data from past tasks to help maintain high accuracy even with data drift. Fundamentally, single-level non-hierarchical EM design cannot have the best of both worlds, i.e., high speed and ample space [35]. HEM addresses the limitations of single-level EM by optimizing it over a deep memory hierarchy. Figure 1 shows the execution stages a new task goes through in HEM.

- **Buffering** **B**: The samples for a new task N are accumulated in a *stream buffer* and later retrieved for training. The size of the task N depends on the learning method in use, which can be either large new class data [43, 58] or simply a small chunk of new samples [17, 50].
- **Training** **T**: HEM combines samples from the task N in the stream buffer with old samples in EM to compose training data. These combined samples are organized into mini-batches, which are then fed into model training one at a time, constituting training iterations. This process can be repeated in multiple rounds, known as epochs, to improve the accuracy of the model.
- **Swapping** **S**: During the training of the task N , HEM swaps data between in-memory samples and in-storage samples of the same class. This is performed asynchronously to prevent slow storage access from delaying the continual model training. In cases where the available I/O bandwidth is insufficient, only a small subset of EM samples are swapped. By default, HEM randomly selects these samples [35].
- **Flushing** **F**: Once the training of the task N is completed, its samples in the stream buffer require EM to be updated with these samples. If EM has no space to store all of them,

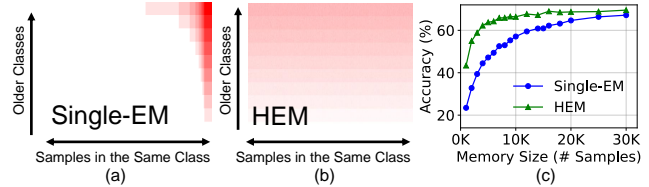


Figure 2: (a) and (b): Data diversity of old samples between single-level EM and HEM. (c): Accuracies over memory sizes.

HEM applies a sampling strategy to reorganize EM with a subset of the task’s samples. Old tasks should also evict some samples to avoid the overflow of EM. The stream data is then flushed onto the storage and cleaned up for the next incoming task $N+1$. We keep both in-memory and in-storage data class-balanced within the capacity.

Data Diversity. In HEM, any samples in storage have an opportunity to be replayed in the future. Thus, more diverse old samples can contribute to better coping with the forgetting of their tasks. Figure 2(a) and (b) illustrate the range of old samples that take part in training between traditional single-level EM design and HEM, respectively, over ten tasks that contain different classes from the CIFAR100 dataset [33]. Figure 2(c) compares the final top-1 accuracy averaged across all classes between the two methods for image classification using the ResNet-32 model [28].

3 DESIGN SPACE EVALUATION

In this section, we analyze the design parameters of HEM to gain a thorough understanding of their impact on both system and model efficiency. Traditionally, these parameters have been configured *statically* to maximize model accuracy for non-hierarchical EM designs [9, 13, 17, 42–44, 58]. However, simply repurposing this static configuration for HEM on edge devices without considering its impact on energy efficiency would not yield practical benefits. Through our study, we offer valuable insights to aid the development of a system runtime for cost-effective HEM.

3.1 Methodology

System Platform. Our study utilizes NVIDIA Jetson TX2 (TX2) [3] and Jetson Xavier NX (Xavier) [4] as reference edge devices. TX2 is equipped with a 256-core NVIDIA Pascal GPU, 8GB of RAM, and a 32GB eMMC 5.1 drive. Xavier is equipped with 384-core NVIDIA Volta GPU, 16GB of RAM, and a 16GB eMMC 5.1 drive. The RAM is a single unified memory shared by the CPU and GPU. To conduct experiments, we adopt CarM [1] that runs on PyTorch 1.7.1 and has been enhanced with the ability to dynamically configure HEM parameters.

Datasets. Table 3 provides a summary of the full datasets used in evaluating Miro. However, for this particular characterization study, we focus on image classification tasks and utilize two popular datasets: CIFAR100 [33] (100 classes,

Parameter	Description	Resource	Decision	Constraint
EM size	# old samples populated in RAM	Memory	Dynamic	Trade-off
SB size	# new task’s samples kept in RAM for training	Memory	Dynamic	Trade-off
Swap ratio	Average % for EM samples to be replaced by other samples in storage	I/O	Dynamic	Capacity
Epoch count	# times the data combining EM and SB is trained upon a new task	GPU	Static	Static

Table 2: Descriptions for four design parameters of HEM. For each parameter, we show HW resource type it exercises, how to make configuration decisions, and the constraint to which it is bounded.

197MB) and Tiny-ImageNet [7] (200 classes, 1.1GB). By default, we split each dataset into 10 tasks, with each task comprising of 10 classes for CIFAR100 and 20 classes for Tiny-ImageNet, guided by many prior works in CL domain [9, 13, 42, 43, 58]. These tasks are issued sequentially and do not overlap, ensuring that each sample appears only once.

While these datasets can fit easily in the RAM of TX2 and Xavier, it is important to note that on-device CL is restricted by energy expenses incurred by training in-memory data (i.e., stream buffer plus EM), rather than by memory usage to maintain the data. In fact, the impact of memory usage is a double-edged sword. For instance, a larger EM may improve accuracy, but it can also increase energy consumption due to the training data that gets larger. This also often results in diminishing returns or even no improved accuracy compared to smaller EMs. Although it is worthy of evaluating gigantic datasets like ImageNet1k [45] (146GB) to demonstrate longer-term effects (§6.2), we urge caution against always *using up* all available memory for sizing stream buffer and EM, irrespective of the dataset in use.

Training Methods. We employ ResNet-32 and ResNet-18 as the reference models for CIFAR100 and Tiny-ImageNet, respectively. To run these models on HEM, we have chosen two CL methods: ER [44] and BiC [58]. ER is a pure episodic memory-based method without any additional algorithmic optimization, whereas BiC incorporates *knowledge distillation*, a widely used CL technique that transfers learned knowledge backward as more tasks are added. For ER, we use the same hyperparameters and loss function (binary cross-entropy loss) as in [43]. The default learning rate is 2.0, and the weight decay is $1e-5$. BiC employs bias correction on the last NN layer to minimize data imbalance between past and new samples. Its loss function combines distillation loss and cross-entropy loss calculated from designated old samples. The default learning rate is 0.1, and weight decay is $2e-4$ and $1e-4$ for CIFAR100 and Tiny-ImageNet, respectively.

Metrics. To measure power consumption, we exploit the built-in sensor values for the GPU, RAM, CPU, and I/O connection between the RAM and storage on the Jetson device [2, 5]. Power is measured in watts (W) and energy is gauged in joules (J) by multiplying power by time. As for the accuracy metric, we calculate the final accuracy averaged across all classes after completing the last task training. This

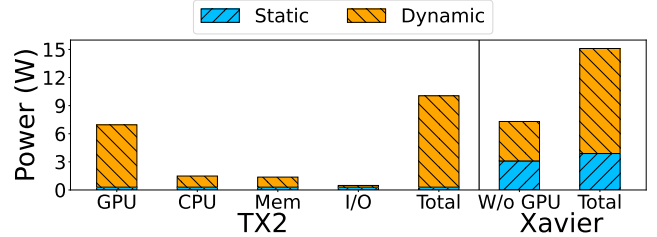


Figure 3: Power consumption of HEM across major system components on NVIDIA Jetson TX2 and Jetson Xavier NX.

final average accuracy has been a standard metric in continual learning used to measure accuracy over consecutive task insertions [9, 13, 42, 43, 58].

3.2 Design Parameters

Table 2 outlines four representative parameters – *EM size*, *stream buffer (SB) size*, *swap ratio*, and *epoch count* – that impact the performance, accuracy, and energy efficiency of HEM. These parameters capture the resource usage required for new task training. In general, higher resource usage leads to higher accuracy. However, each parameter has unique implications on cost-effectiveness, which refers to the accuracy improvement achieved for the energy spent. For example, more epochs consume energy proportionally but only offer minimal accuracy improvement once the model converges, resulting in low cost-effectiveness.

It is worth noting that each parameter exercises specific HW resources within the system. EM and SB operate on RAM, data swapping mainly involves I/O operations, and epoch count pertains to GPU usage for model training. This also means that certain parameters may compete for the same resources when capacity constraints arise. For instance, the GPU is exclusively dedicated to model training, whereas I/O bandwidth is a system resource that varies in its availability as all on-device programs carry out I/O operations. Our system runtime will be designed to adapt to these interferences based on the observations made in this study.

3.3 Energy-Accuracy Characteristics

3.3.1 Impact on System Power. Compared to other methods, HEM exercises more system resources: e.g., traditional EM methods do not operate I/O for data swapping and non-EM methods do not even manage memory for replaying. Therefore, it is crucial to understand the power characteristics of HEM that arise from changing parameter values.

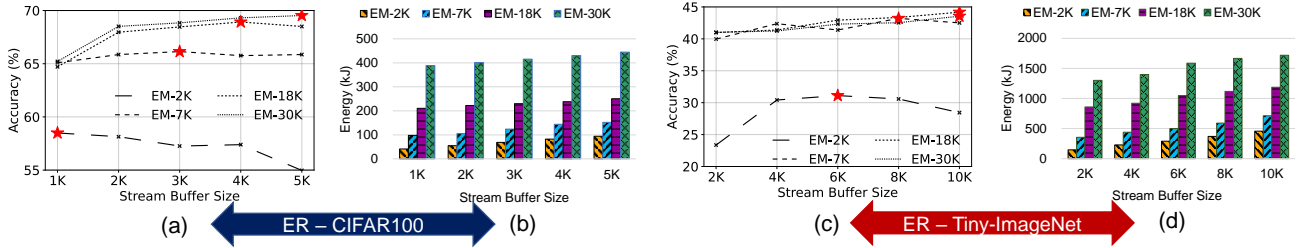


Figure 4: (a) and (c): Accuracy over varying SB sizes and EM sizes in terms of the number of samples for CIFAR100 and Tiny-ImageNet. (b) and (d): Their corresponding energy consumption.

For this analysis, we run the HEM using CIFAR100 and ER with full data swapping, *i.e.*, 100% swap ratio, on both TX2 and Xavier, using default power modes with a power budget of around 10W for TX2 and 15W for Xavier. Figure 3 illustrates power consumption by distinguishing between static and dynamic power to precisely confirm the impact of training. We make three observations. (1) Dynamic power dominates, resulting in the total power consumption nearly reaching the power budget for each device. (2) Among system components, the GPU is responsible for most dynamic power consumption. While TX2 reports the GPU power separately, Xavier reports a single number for all on-chip components. To determine the effect of GPU dynamic power, we make the GPU consume only static power by inactivating it during the training process, which is shown in the w/o GPU. We found that the GPU dynamic power still accounts for up to 42.7% in Xavier. (3) I/O activity driven by data swapping accounts for a small portion of the power consumption (~0.1W). Even when we saturate I/O bandwidth, I/O power usage does not increase its portion significantly. Our findings are summarized in the first row of Table 1.

3.3.2 Design Parameters. **Memory Parameters: EM and SB.** Now, we uncover the energy-accuracy trade-off associated with each design parameter by studying its impact on the training time and prediction accuracy of the model. To begin, we focus on two memory parameters: EM and SB.

We explore EM and SB for different pairs of sizes and show the accuracy and energy usage in Figure 4 for CIFAR100 (a/b) and Tiny-ImageNet (c/d) using ER. BiC exhibits similar trends, so we omit it for brevity. Each accuracy figure of (a) and (c) includes a set of lines, with each line representing the changes in accuracy for a particular EM size over different SB sizes on the x-axis¹. The energy property in (b) and (d) is easy to depict – More energy is consumed for operating larger memory that combines more EM and SB samples. Then, the question remains whether it is cost-effective to use larger memory for EM and SB.

¹Note that the task size of CIFAR100 and Tiny-ImageNet is 5K and 10K. If the SB is smaller than the task size, some remaining samples are not stored in SB but are still kept in storage and retrieved later for replay.

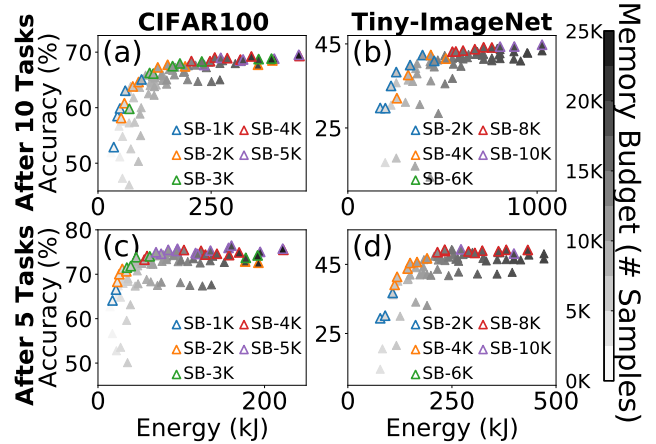


Figure 5: Energy-accuracy trade-offs over varying memory budgets shared by EM and SB.

For the same EM size, increasing the size of SB does not necessarily improve accuracy. In many cases, the highest accuracy is achieved when the SB size is smaller than the maximum value on the x-axis. This phenomenon significantly harms energy-sensitive edge devices because a larger SB directly leads to longer training time and higher energy spending. The red symbol \star on each accuracy graph indicates the SB size that produces the best accuracy for the same-sized EM. The optimal SB size often differs.

We observe a similar trend when adjusting the EM size for the same-sized SB, *i.e.*, the same x-axis value. Specifically, for both CIFAR100 and Tiny-ImageNet, we see no noticeable improvement in accuracy when the EM size increases from 18K to 30K. A bigger EM also leads to increased data swapping and I/O operations due to more EM samples drawn for training. However, the I/O power consumption is insignificant relative to the GPU power, so an enlarged data-swapping activity does not contribute to higher energy consumption.

EM and SB as One. From Figure 4, it is evident that effectively allocating a given memory budget across EM and SB is a challenging task. To further demonstrate this, we show the impact of different EM and SB size pairs on energy and accuracy while varying the memory budget in Figure 5(a) and (b). Each data point is represented by various shades

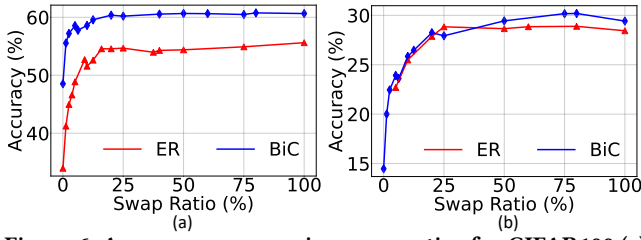


Figure 6: Accuracy over varying swap ratios for CIFAR100 (a) and Tiny-ImageNet (b).

of gray based on the memory budget, with darker shades indicating higher memory budgets. We also highlight the color of the SB size that produces the best accuracy out of all possible size pairs that split the same memory budget. We make three observations. (1) Bigger memory budget still does not guarantee higher accuracy. (2) The best SB size differs across memory budgets. (3) Blindly committing full capacity Δ to SB to emphasize “learning a new task” over “remembering old tasks” is not always necessary.

The current approach to allocating memory *prioritizes* SB over EM to enable all new samples to be used for training [42, 43, 58]. This approach is reasonable for non-hierarchical EMs, where only a small subset of samples from an old task can be stored in EM and participate in replaying later. However, HEM maintains a much larger number of old samples in storage, allowing for more effective replay. This is presumably the main reason behind the second observation. We observe no static memory pair that aces across NN models, datasets, and problem sizes, which renders static or history-based memory-sizing strategy ineffective. For example, Figure 5(c) and (d) show accuracies right after the training of five tasks. The best accuracy for each memory budget is vastly different compared to Figure 5(a) and (b). These findings are summarized in the second row of Table 1.

I/O Parameter: Swap Ratio. Figure 6(a) and (b) show the impact of the swap ratio on model accuracy for ER and BiC with an EM size of 2K, using CIFAR100 and Tiny-ImageNet datasets, respectively. We see that even a tiny swap ratio can remarkably improve accuracy compared to traditional non-hierarchical EM setups, which correspond to a swap ratio of zero. Overall, the accuracy increases sharply from 0% to 20% and then plateaus. We observe this trend is fairly consistent across EM sizes.

Notice that HEM’s I/O operations are asynchronous and incur virtually zero delay to training time [35]. Moreover, the required I/O bandwidth for full swapping, where every EM sample is swapped every epoch, is only 3.8MB/s for CIFAR100 and 16.8MB/s for Tiny-ImageNet, which are well below the I/O bandwidth provided by removable storage devices like MicroSD cards. Faster mobile GPUs that can train models faster may put more strain on I/O traffic. However, due to the insignificant impact of I/O on system dynamic

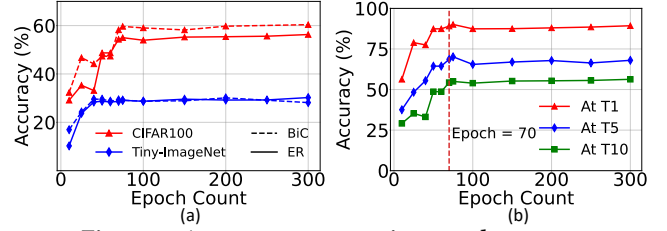


Figure 7: Accuracy over varying epoch counts.

power (*i.e.*, 0.1W for 100% swap ratio), faster mobile GPUs are unlikely to exacerbate I/O power in the near future. So, improving model accuracy with higher swap ratio is nearly cost-free. This claim is also factored in the first row of Table 1.

GPU Parameter: Epoch Count. The system consumes energy proportional to the epoch count. Typically, for both ER and BiC, accuracy reaches a plateau after a certain number of epochs, as shown in Figure 7(a). This indicates that a statically configured epoch count is feasible. Then, a key question is whether we can terminate training for each task earlier to save energy. To see the possibility, we explore the accuracy observed after training the first, second, and last tasks using different epoch counts. For brevity, we present the results for ER on CIFAR100 in Figure 7(b). The vertical line indicates the epoch count of 70, a hyperparameter suggested by prior work [35]. The number of epochs required to reach convergence remains almost identical at around epoch 70. Reducing the number of epochs for intermediate tasks has negatively affected subsequent tasks. Therefore, we consider using the value proven to work well without any adaptation. This is the last insight we describe in the third row of Table 1.

4 MIRO: SYSTEM RUNTIME

We develop a system runtime, Miro, to showcase how our insights for HEM can be leveraged. Miro focuses on optimizing the dynamic parameters defined in the second rightmost column in Table 2. Specifically, Miro accomplishes two critical missions for cost-effective HEM while adhering to device-specific resource constraints:

1. *Selecting data swapping strategy.* The swap ratio is a capacity-bound parameter that has a relatively minor impact on overall energy expenditure. Thus, Miro sets a swap ratio that attempts to fully utilize the available I/O bandwidth. To achieve the goal, Miro continuously monitors system-wide I/O usage to refine the data swapping strategy.

2. *Deciding stream buffer and EM sizes.* The optimal combination of SB and EM, which exhibits high cost-effectiveness, differs across memory budgets and tasks.

Thus, Miro dynamically sizes both SB and EM in the presence of consecutive new tasks within the memory budget. As discussed, using more memory incurs higher energy costs but does not necessarily guarantee higher accuracy. This makes accurately sizing SB and EM even more crucial.

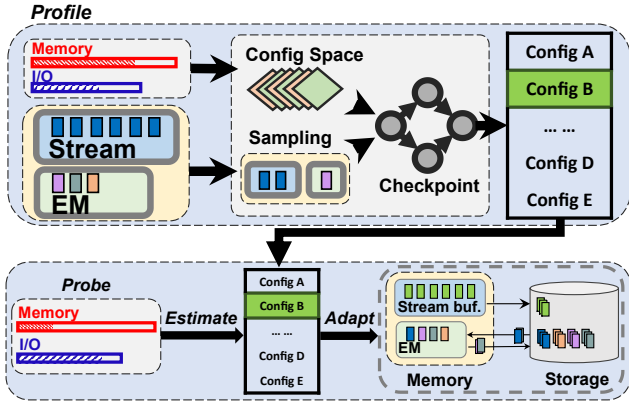


Figure 8: Miro system runtime architecture.

4.1 Design Overview

Although the two missions outlined above are seemingly independent, we strive to integrate them into a unified workflow that operates through a well-defined state machine. This approach allows us to optimize individual parameters without disrupting other aspects of runtime execution. Here, we describe Miro’s operational phases as shown in Figure 8:

- **Profile:** When a new task is ready, Miro conducts profiling by focusing on those parameters constrained by cost-efficiency, i.e., SB and EM. This profiling involves searching for various size pairs of these two components based on possible memory allocations within a memory budget. For each size pair, Miro records an estimate of accuracy and energy usage associated with using it for the new and old tasks.
- **Probe:** At the end of every epoch, Miro probes system resource states to see whether any parameters need reconfiguration. Miro focuses primarily on I/O and memory states for data swapping and SB-EM sizing, respectively, and enters Estimate phase if a state change is identified: e.g., I/O becomes congested or memory budget is updated.
- **Estimate:** Miro computes new parameter values for the state change occurring at the target resource. It computes a new swap ratio for I/O congestion or new SB-EM sizes for a new memory budget. Then, Miro enters Adapt phase.
- **Adapt:** Miro refines the target parameters with the values derived from Estimate phase. Once this refinement is complete, Miro re-enters Probe phase.

Miro carries out profiling of SB and EM at every task insertion, requiring it to be done at low overhead. While there are other approaches to avoid repetitive profiling, such as relying on static configurations or historical data, we have opted *not* to pursue them for the following reasons:

Why Not Using Static Configurations? A static configuration often produces the best outcome when recurring training jobs in an offline setup start from the same initial condition [60], i.e., a fresh model with no observed data.

However, in continual learning, each task begins training from a distinct condition due to the accumulation of model updates over time and data drift occurring among tasks. Thus, a configuration that yields optimal results for the current task may not produce the same outcome for the next tasks.

Why Not Using Configurations from History? An incoming task T_i may resemble an old task T_j , where $j \neq i - 1$, thereby tempting us to reuse the same configuration that was previously used for T_j . However, despite the similarity between the stream samples of T_i and T_j , the samples in EM may differ significantly. In other words, the knowledge that the model must retain upon the availability of T_i as compared to T_j may be markedly different. So, we cannot guarantee that a previously successful configuration will be effective for similar tasks in the future.

4.2 Data Swapping Strategy

The strategy for data swapping in Miro is designed with three properties in mind:

- P1) I/O energy consumption is insignificant.
- P2) Increasing the swap ratio provides benefits across a broad range, with a knee point appearing at a relatively low swap ratio (15–20%) in the ratio-accuracy curve, as demonstrated in Figure 6.
- P3) Other programs running on the device can abruptly compete for I/O resources. But, under normal circumstances, HW typically allows training jobs to leverage ample bandwidth for full-fledged data swapping.

Tuning Swap Ratio. P1 allows us to focus on a single knob, I/O usage. When I/O is idling, we increase the ratio *incrementally* by a small discretized value (default 10%), taking advantage of the benefits highlighted in P2. Conversely, when I/O is congested, we decrease the ratio by a large quantity (default half) to *quickly* alleviate I/O contention, based on P3. Despite the ratio that decreases rapidly, we can maintain an effective swap ratio even after a few times of congestion handling, i.e., 100% → 50% → 25%, without reaching the knee point. The techniques we use to adjust the swap ratio based on I/O contention or idleness are skin to those employed in TCP congestion control [22, 26]. All this process is performed by Estimate phase.

Obtaining I/O State. During Probe phase, Miro performs system I/O queue monitoring to determine the state of HEM, which can be classified as one of three states: *Congested* when the I/O queue experiences back-pressure; *Idle* when the I/O queue remains empty for longer than a predefined duration of time; and *Stable* when the I/O queue is neither congested nor idle. If I/O is idle or congested, Miro forwards the observed state to Estimate phase, which in turn triggers the adaptation of the swapping ratio to react to the state.

Reducing Swap Ratio. Miro reduces the swap ratio by first increasing the swap interval. We found that updating the interval value is beneficial for swap ratios ranging from 100% to 20%, which corresponds to a value range of 1 to 5 epochs. However, for swap ratios below 20%, we maintain the interval fixed at 5 epochs and adjust the swap percentage adequately to achieve the desired target swap ratio.

4.3 Stream Buffer and EM Sizes

Now, we explain how Miro configures two memory parameters, SB and EM, that significantly influence both accuracy and energy efficiency. The sum of their sizes should not exceed the memory budget, which we assume to be user-specified by system admins.

4.3.1 Memory Parameter Optimization Problem. Miro must reduce the strain on small battery-powered devices that require high energy efficiency while delivering high-accuracy models to satisfy user experiences. Between energy efficiency and accuracy, which are often at odds with each other, we assume accuracy takes precedence over energy efficiency. Therefore, our ultimate objective is to identify an optimal configuration for SB and EM sizes, or *conf* for brevity, that conserves energy while maintaining high accuracy. Since the definition of high accuracy can be subjective, Miro provides users with an implicit method called *cutline* to aid in determining its appropriate magnitude.

4.3.2 Design Insights through an Example. Numerous algorithms exist for optimizing memory parameters. To compare these algorithms and explain the rationale behind our choice, we use a simplified example borrowed from real profiling as shown in Figure 9. This example includes a list of confs along with their respective accuracy and energy consumption in training the current model with each conf. Later in this section, we will discuss our profiling method for acquiring this information at low costs.

Why Not Using a Single Metric? Consider methods that select a conf using a single metric, either energy efficiency or accuracy. The most energy-efficient conf in Figure 9 is (0.5K, 0.5K) for (SB, EM). In this case, the achieved accuracy is far below what we believe as good accuracy shown in the list. Similarly, the conf that delivers the highest accuracy is (5K, 10K) that can store up to 15K samples in total, making it the highest energy-consuming option. However, if we examine confs with similar accuracy levels, e.g., within 2%, we can find a more energy-efficient option that requires only 3K samples, the conf (1K, 2K). This conf requires around 20% of GPU energy compared to the 15K-sample conf. We commonly encounter similar problems when dealing with many lists of memory confs using a single metric.

(EM, SB)	(Acc, Energy, Utility)
(5K, 10K)	(71.2, 23.5, 3.0)
(1K, 2K)	(69.8, 4.2, 16.6) HU + Cutline
(1K, 1.5K)	(54.2, 3.3, 16.4) LE + Cutline
...	...
(1K, 0.5K)	(46.0, 2.4, 19.2)
(0.5K, 0.5K)	(45.0, 1.4, 32.1) HU Only

Figure 9: An illustrative example of how our method works. HU: highest utility. LE: lowest energy.

Simply Combining Two Metrics is Enough? To account for both metrics simultaneously, we propose a new metric called *utility*, which represents the accuracy gained per unit of the energy spent²:

$$\text{Utility} = \frac{\text{Accuracy Gain}}{\text{Energy Usage}} \quad (1)$$

Therefore, the conf with the highest utility is the one that spends energy most efficiently to improve accuracy.

Figure 9 shows that the conf (0.5K, 0.5K) has the highest utility. To maintain good accuracy in this round of task training, however, one might choose the conf (1K, 1.5K) or the conf (1K, 2K) instead of the conf (0.5K, 1K), as both are considered energy-efficient among all candidates. This highlights that merely considering utility, although both energy efficiency and accuracy are factored in, falls short of meeting our fundamental requirement of achieving “high accuracy”. To reach our objective, we need to first exclude unpromising confs attaining low accuracy.

4.3.3 Our Method. We introduce *cutline*, a straightforward yet powerful technique that enables us to narrow down high-accuracy confs by their accuracy ranks. For instance, if we apply a cutline of 20% to our example in Figure 9, we can obtain the candidate subset that comprises 20% of the confs (colored region) with accuracy higher than the other 80% that the cutline has filtered out. On top of this, if we search for the conf with the best utility, we obtain the conf (1K, 2K), which is a valid choice. Interestingly, we can even apply a single metric “energy efficiency” after the cutline and obtain a good conf (1K, 1.5K). This is because the cutline already sifts out candidates that satisfy our high-accuracy criterion.

Using an appropriate cutline is undoubtedly crucial, and this involves a trade-off. A tighter cutline will leave fewer confs with higher accuracy, thereby increasing the likelihood of selecting a conf that consumes more energy. Based on empirical studies, we found that a cutline range of 20–50% works well in practice.

²We tested various utility score designs, including those based on curve-fitting and stochastic approximation. However, they either proved to be computationally expensive or did not outperform our current design.

Nonetheless, in scenarios where a very slight margin from the maximum possible accuracy is permitted, Miro can dynamically determine the cutline to identify a small group of confs with exceptionally high accuracy. It is important to note that larger memory usage does not guarantee higher accuracy, and achieving the highest accuracies over task insertions requires different memory allocations for old and new samples. Miro addresses these challenges, regardless of the cutline value in use.

4.3.4 Profiling at Low Overhead. The goal of profiling is to build a fresh list of confs to examine for every task insertion. Profiling should be lightweight so that its energy expenses do not outweigh the benefits gained from executing a cost-effective conf selected by Miro. Naïve profiling entails model training on many different SB and EM sizes for many epochs and samples, which lead to prohibitively high energy costs. As such, we strive to minimize profiling overheads from two angles: (A1) number of confs and (A2) single-conf evaluation time. We follow several popular guidelines:

- A1)** Avoid exhaustive profiling that covers all size variations. Profile a small subset of confs.
- A2.1)** Do not use the entire training data that include all stream buffer and EM samples. Use a subset of the data.
- A2.2)** Do not go through all epochs. Perform training for a small number of epochs and infer the accuracy that could be obtained if there were many more epochs.

While there are common conventions taken to tackle these issues, they do not work very well on our problem or should be used with caution:

Reducing # Confs (A1). Several algorithms or heuristics [11] exist to narrow down the search space. The idea behind them is to identify unpromising confs in history and exclude the search range that covers those confs. However, in CL setups, confs from the past may not provide much insight into their significance in the future due to the similar reason explained in §4.1. Therefore, we opt for a safer approach of reducing the number of confs by uniformly sampling instances from the space.

Reducing # Training Samples (A2.1). We rely on random sampling to reduce training samples, as it is well-known for preserving the distribution of original data in CL setups [11, 35]. On top of it, we meticulously verify if the sampling rate in use covers samples across all classes. Otherwise, the classes not represented in the samples will report zero accuracies, causing misleading results.

Reducing # Epochs (A2.2). We obtain the accuracy of each conf by running a few epochs and use the observed accuracy without extrapolating to the final accuracy of the model. In general, confs that achieve higher accuracy when processed until convergence tend to have a steeper accuracy increase

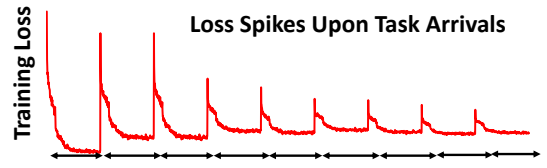


Figure 10: Constant spikes and noises in training loss when training new tasks.

Dataset	Classes	Tasks	Samples	Size	Task Domain
CIFAR100	100	10	50k	197MB	Image Classif.
Tiny-ImageNet	200	10/20	100k	1.1GB	Image Classif.
UrbanSound8K	10	10	8732	184MB	Audio Classif.
DSADS	19	10	9120	163MB	HAR
ImageNet1k	1000	50	1.28m	146GB	Image Classif.

Table 3: Datasets used in §3 and §6. We cover three task domains: Image Classification, Audio Classification, and Human Activity Recognition (HAR).

during an earlier training phase. So, the accuracy observed through several training epochs is just informative enough for us to apply a cutline, rank confs, and measure utilities.

However, one major challenge we face is deciding an appropriate time to collect the accuracy data. We have observed that during the earlier epochs, the model tends to exhibit spiky and noisy patterns in training loss that do not reveal any useful information about the accuracy trend across new and old tasks. Figure 10 illustrates this phenomenon. It is only after the first few epochs that the model begins to smoothly improve loss values for both new and old tasks in harmony. Therefore, we take a model checkpoint from a reference conf that has reached a stable point and use it to profile all confs. More importantly, this approach saves on profiling costs tremendously because it eliminates the need to navigate through the earlier phase for each conf.

4.3.5 Tying All Together in Miro Workflow. During Profile phase, Miro selects a set of random confs (default 14 confs) that can fit in the memory budget. It then creates a checkpoint model using a baseline conf borrowed from prior work [35, 43]. Using the checkpoint, each conf runs for a few epochs (default 5 epochs) on a small subset (default 5%) of training data. After all confs are evaluated, Miro applies a cutline and selects the conf with the highest utility. At the end of every epoch, Miro invokes Probe phase to detect if the memory budget is updated. Since the conf selected by our method does not typically harness the full memory budget, SB and EM sizes do not need to be reorganized every time. Only when the current memory usage exceeds the new budget, Estimate phase selects the conf with the highest utility from previously profiled results (without re-profiling) while excluding those confs that the new budget cannot serve. If the budget increases, Miro performs profiling in the next task to avoid excessive profiling. Finally, Adapt phase reconfigures SB and EM based on their new parameter values.

5 IMPLEMENTATION

Built atop CarM [1], Miro extends three key components:

Episodic Memory. Miro implements EM through shared memory using the Python Multiprocessing module [6] to enable direct reads and writes on a shared address space. These accesses are not serialized nor synchronized for high speed, so they can interfere with each other in the same memory location. We ignore this for two reasons: (1) rare event and (2) no visible effect on the statistical model efficiency.

Monitoring. Instead of directly consulting with the OS on I/O status, Miro probes the completion rate of recent data swapping as a proxy of I/O congestion or idleness. This approach reduces monitoring costs. When the swap ratio is reconfigured, Miro informs the swap worker in CarM to change the swapping strategy. The swap worker is also notified of any newly configured EM addresses and sizes.

Profiling. Miro constructs a conf search space by taking into account the new task size and the current memory budget. It then launches mini-training tasks to quickly obtain accuracy and energy estimates for each candidate conf. To avoid frequent SB or EM buffer resizing during profiling, Miro masks the buffers when the target size is smaller than the current buffer size. This is the common case with the sub-sampled buffers used in profiling.

6 EVALUATION

Our experimental setup builds upon the methodology described in §3.1, with several additional benchmarks outlined in Table 3. (1) **Audio Classification:** We use ResNet-18 on the UrbanSound8k dataset [8], which contains 8,732 urban sound files categorized into 10 classes. The sound files are transformed into log-mel spectrograms following the approach in [46]. The dataset is split into 10 single-class tasks. (2) **Human Activity Recognition:** We use ResNet-18 on the Daily and Sports Activities dataset [10], which contains 9,120 motion sensor data samples covering 19 daily and sports activities. The dataset is split into 10 tasks, with tasks 1 to 9 having 2 classes and task 10 having 1 class. (3) **Large-scale Image Classification:** We organize the ImageNet1k dataset into 50 tasks, denoted as ImageNet1k-50Tasks, with each task comprising 20 classes.

In addition, we revise the Tiny-ImageNet to test 20 tasks for a longer sequence, with each task comprising 10 classes, while the CIFAR100 remains with 10 tasks. We use ER as the reference model since HEM makes it optional to use sophisticated algorithmic optimizations. All experiments are conducted on Jetson Xavier NX³. By default, our system

³For ImageNet1k-50Tasks, we perform extrapolation to a larger-memory device by utilizing a server with more memory capacity to faithfully evaluate this demanding dataset, assuming Miro operates on a higher-end edge device with similar energy properties.

consistently consumes 4.7–6GB memory: 2GB for system bootup and 2.7–4GB for running CL methods in PyTorch on unified memory shared by the CPU and GPU.

Competing Methods. Since CarM is the only existing method that exploits memory hierarchy for CL, we have additional baselines and cover strategies that incorporate better static confs, historical data, and heuristics. (1) CarM employs static confs as suggested by [35]. (2) BestStatic explores all possible static confs and finds the conf that offers the best cost-effectiveness, guided by a cutline and the highest utility or lowest energy. This is intended for us to see the (almost) best possible outcome for using static confs. (3) BestHistory selects the best intermediate conf identified by BestStatic after completing half of the tasks and uses the conf for future tasks. (4) Heuristic treats new and old tasks equally and assigns memory to EM vs. SB proportional to the number of tasks placed in each component. The motivation behind this is that HEM can replay old data very effectively. For a fair comparison, we assume all methods perform full-fledged data swapping unless otherwise specified.

We adopt a step size of 0.5K samples for memory sizing, which is sufficiently fine-grained. In reality, BestStatic and BestHistory require exhaustive exploration of numerous static confs, but we exclude the exploration cost for these methods to focus on showing their potentially best-case efficacy. However, we include the profiling overhead in Miro to avoid over-emphasizing our effectiveness. We will show that despite this overhead, Miro outperforms the other methods.

6.1 Main Results

We begin our experiments by evaluating all competing methods on medium-scale datasets from Table 3 in two steps. First, we compare Miro with CarM, BestStatic (BS), and BestHistory (BH), which represent static strategies. Second, we compare Miro with Heuristic to focus on dynamic strategies. A naïve Heuristic (Heu) always uses up the entire memory budget, so it clearly hurts energy efficiency. Therefore, we will allow Heuristic to consume a portion of the memory budget, enabling it to trade off accuracy for energy saving.

Comparing to Static Methods. To perform a faithful comparison of these competing methods, we vary memory budgets over the datasets and draw energy-accuracy trade-off graphs in Figure 11. For Miro, BestStatic, and BestHistory, which employ a cutline, we set it to 50% and show the conf choices from both the highest utility (HU) and lowest energy (LE) perspectives. In each graph, the x-axis represents energy usage (lower is better), and the y-axis represents accuracy (higher is better). Cost-effective methods will choose confs that conserve energy while maintaining high accuracy, appearing closer to the upper-left corner of the graph than less cost-effective, less desirable ones. Overall, Miro consistently

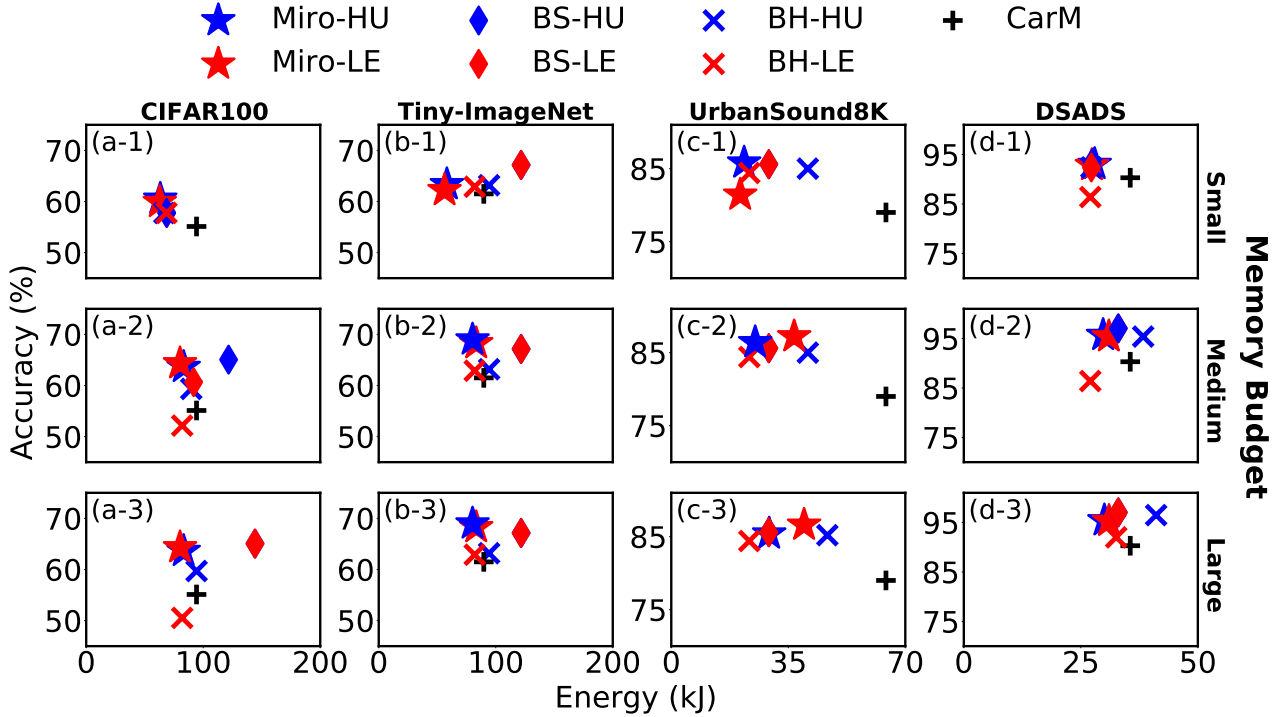


Figure 11: Energy-accuracy trade-offs over competing static methods for a combination of different datasets (a-d) and memory budgets (1-3). For example, the subgraph (a-1) compares the methods using CIFAR100 on a small memory budget. The memory budgets are 10K, 25K, and 50K for CIFAR100 and Tiny-ImageNet and 1K, 2K, and 2.5K for UrbanSound8K and DSADS.

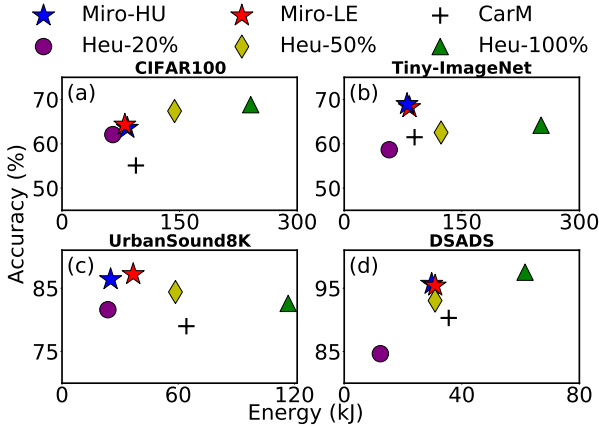


Figure 12: Energy-accuracy trade-offs between Miro and Heuristic over different datasets at the medium memory budget used in Figure 11.

outperforms or is on par with other methods, demonstrating superior cost-effectiveness.

It is worth comparing Miro with CarM, the state-of-the-art HEM design based on static parameters, in detail. Compared to CarM, Miro uses 23–66% less memory while achieving 1.35–9.19% higher accuracy across benchmarks and memory budgets. Overall, we see higher effectiveness when larger memory budgets are available for Miro to use. This is because

our runtime profiler can cover a wider spectrum of EM and SB sizes and determine more effective confs that can be found in larger memory budgets.

Miro, in particular Miro-HU, tends to make better choices than BestStatic and BestHistory, even without including their prohibitive exploration costs in the graphs. Occasionally, they provide confs with slightly better accuracies but at significantly higher energy usage. BestHistory is less effective than BestStatic even though they both require exploration to find out the best static conf. This indicates that previously successful confs may not be effective for future tasks. To summarize, Miro achieves its goal of striking a good energy-accuracy trade-off across memory budgets.

Comparing to Dynamic Methods. For Heuristic, we vary the amount of in-use memory in order to avoid always utilizing a given memory budget, as shown in Figure 12. When Heuristic fully utilizes the given memory, it provides an accuracy improvement of only 4.45% for CIFAR100 and 2.24% for DSADS, while consuming three times more memory on average than Miro. This trade-off is not considered worthwhile. For UrbanSound8K and Tiny-ImageNet, Miro outperforms Heuristic in accuracy by 4.6% and 4.04%, respectively. When we limit Heuristic to use 20% (Heuristic-20%) or 50% (Heuristic-50%) of the given memory budget, it occasionally achieves comparable cost-effectiveness to Miro. However,

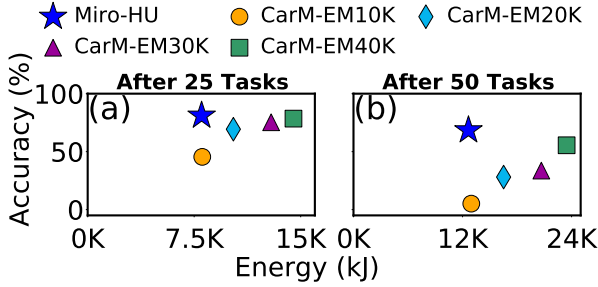


Figure 13: Energy-accuracy trade-offs after completing 25 tasks (a) and 50 tasks (b) for ImageNet1k-50Tasks.

determining the best way to leverage partial memory is also a search problem, which we solve elegantly in Miro.

6.2 ImageNet1k-50Tasks

In the CL literature, ImageNet1k has commonly been evaluated as a sequence of 10 tasks, each consisting of 100 classes with 1,300 samples per class. However, longer task sequences better represent more realistic use cases where edge devices require frequent, real-time model updates. Thus, our evaluation with ImageNet1k is based on 50 tasks, with each task including 20 classes. Due to prohibitive cost of fine-grained exploration in BestStatic and BestHistory, we focus on comparing Miro with four static confs based on CarM with varying EM sizes: 10K (CarM-EM10K) to 40K (CarM-EM40K) samples, which cover the energy-accuracy trade-off spectrum. For Miro, we use the highest utility (HU) as the conf selection metric.

To highlight how Miro behaves in the lengthy task sequence, we present energy and accuracy after completing 25 and 50 tasks in Figure 13. Miro consistently outperforms all 4 static confs in terms of cost-effectiveness in both task completion points. Importantly, the performance gap between Miro and CarM widens as more tasks are trained. For instance, Miro and CarM-EM20K maintain similar utility until 10 around tasks, but after 25 tasks, Miro exhibits 45.7% higher utility, which further increases to 218.63% after 50 tasks. This is expected because static memory confs cannot adapt to the varying task properties, which become more evident in longer task sequences.

6.3 Design Validation

For design validation, we utilize Miro-HU for ResNet-32 training on CIFAR100 with a memory budget of 25K samples. **Profiler Optimizations.** We compare four profiler variations to assess cost-reduction techniques. (1) None performs exhaustive search and full profiling without any cost reduction. (2) Conf reduces the number of confs to explore to 20% (14 confs). (3) Conf+Sample adds sub-sampling of training data (5%) on top of Conf while still profiling full epochs.

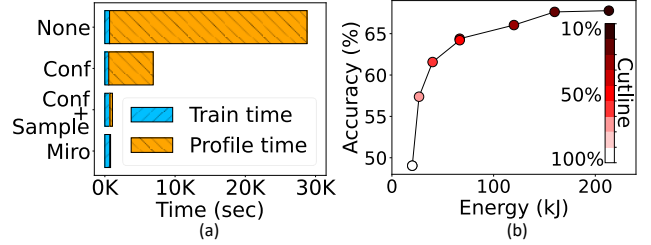


Figure 14: (a) Time breakdown for various profilers with and w/o cost-reduction optimizations. (b) The memory-accuracy trade-off results of different cutline values.

The results in Figure 14(a) demonstrate profiling time and model training time, which combined constitute the end-to-end time. We make two observations. First, profiling costs decrease as we add cost-reduction techniques one by one, making the profiling cost of Miro 346 \times faster than None. Second, the confs chosen from these profilers do not significantly increase model training time, making Miro the most effective in balancing profiling time vs. model training time. Hence, our main features greatly contribute to Miro’s system performance. Furthermore, we observe that all profilers achieve competitive accuracies (62.07–63.48%), suggesting that other profilers do not offer good cost-effectiveness.

Checkpoint. Using checkpoint avoids collecting unreliable profiling results during the earlier epochs, where spikes and noises in the training loss appear. To confirm the effectiveness of this approach, we compare our method to the method without checkpoint: Epoch-15, which runs 15 epochs from epoch zero. Note that our method takes a checkpoint at epoch 10 and runs each conf for 5 epochs to finish it at epoch 15. We compare profiling time and accuracy. Our method achieves comparable accuracy (0.26% less) to Epoch-15 while reducing profiling costs as much as 70%.

Cutline. To properly filter out unpromising confs, Miro relies on an appropriate cutline value. Thus, we evaluate a wide range of cutline values from 10% to 100% (*i.e.*, no cutline) and present the energy-accuracy trade-off results in Figure 14(b). A cutline of 80–100% leaves too many unpromising confs, increasing the risk of accidentally selecting a conf with low accuracy but high utility due to very small memory usage (as shown in our example in Figure 9). We found that setting the cutline between 20–50% works well for our benchmarks, while Miro could further improve its adaptability by adjusting the cutline based on the current accuracy distribution.

7 DISCUSSION

Storage Lifespan and Capacity. MLC-based SD cards today endure around 10,000 write-and-erase cycles. Miro writes samples to storage only once per task, with later data-swapping operations involving only reads. Thus, with proper wear leveling, Miro will not significantly harm the storage lifespan.

However, when scaling up to a very large number of tasks, realistic on-device CL based on HEM may exceed the storage capacity. In such cases, there are two possible options. One option is to embrace larger external storage in edge servers or cloud services, which may require an additional level of data privacy. The other option is to evict some in-storage samples from each class to make room for accommodating more data, which may require a good data sampling strategy. In either case, a good data selection strategy for a deeper memory hierarchy will be needed.

Temporal Data Locality. Consider video analytics as an example. On-road or urban videos have high temporal locality, requiring NN models on edge devices to focus on recent object appearances and classes: unrelated objects may not be the target of inference. In other words, the NN models may need to be customized to a specific distribution of objects at any given time. To enhance the effectiveness of HEM for this particular scenario, we can allow it to use in-storage data collected from recent tasks more aggressively by increasing their swapping activity and EM space. To do this, Miro needs to be improved with more fine-grained, task-level resource allocation policies for both memory and I/O.

Profiling. Our evaluation datasets are structured to reveal data drift between two adjacent tasks, making performing a search each time a task is added a natural choice. Nonetheless, there may be more efficient approaches for certain workloads like video analytics, where consecutive tasks defined by fixed time windows often exhibit high temporal locality and similar class distributions [11, 32]. In such cases, it may be possible to treat two adjacent tasks as a single, larger task that does not require parameter reconfiguration.

Energy-efficient Training Iterations. Most of the energy consumption in on-device CL comes from GPUs that execute training iterations. This highlights the potential effectiveness of strategies like layer skipping [30], layer freezing [59], and sparsity-aware training [52, 56] in improving the energy bottleneck of GPUs by reducing the computational costs of training iterations. These optimization techniques are complementary to Miro’s approach, which enhances energy efficiency by reducing the total number of SB and EM samples required for training. By combining both approaches, we can make on-device CL even more energy-efficient.

8 RELATED WORK

One of the most realistic CL scenarios is class-incremental learning (CIL), which involves inference without task IDs [23]. We focus on EM-based methods for our study since they tend to show better accuracies in CIL [42].

Episodic Memory Management. Several works aim to improve the quality of EM samples through various methods, such as storing samples that represent the mean and

boundary of each class distribution [37], generating a core-set [12], perturbing styles of remembered samples using GANs [20], and promoting the diversity of samples in EM [9]. These methods may involve excessive computation or difficulty [12, 20]. However, most of these methods show only marginal accuracy improvements over uniform random sampling [14, 15, 43]. Some works propose to directly generate samples of past tasks [29, 48, 51, 57]. Unlike these works addressing sampling efficiency, the focus of this study is on devising system-oriented techniques that smartly manage samples across the memory-storage hierarchy.

Recently, BudgetCL [41] introduced a single-level EM architecture based on storage. It utilizes uniform sampling from EM to limit training within a predefined computational budget. While BudgetCL can serve as a replacement for HEM, it may face training slowdowns due to frequent I/O operations, as demonstrated by the CarM work [35]. Nevertheless, Miro can be adapted to work with BudgetCL’s memory architecture for cost-effectiveness since the variation in trained EM samples in BudgetCL corresponds to data swapping within the storage. This results in minimal impact on the system’s energy consumption, as inferred by Figure 3.

Continual Learning on the Edge. There are a few noteworthy works done for improving CL on the edge. Hayes *et al.* [27] explore seven online CL methods that train one sample at a time using CNN models designed for embedded devices, providing algorithmic guidance in this area. Kwon *et al.* [34] compare the trade-offs between performance, storage, and compute and memory costs for regularization vs. EM methods. They observe that EM methods like iCARL [43] offer the best performance trade-offs. Some of their claims emphasize the need for system approaches to improve EM methods, which is aligned with our research goal.

Offline Learning on the Edge. Several recent system studies also focus on the memory and energy efficiency of on-device learning under conventional non-CL setups. Sage [24] performs operator- and graph-level optimizations at compile time and memory management, such as gradient checkpointing [25], at runtime for memory-efficient training. Melon [54] optimizes model training performance under a given memory capacity by leveraging micro-batch [31] and recomputation [19] techniques. E²-Train [55] cares about both training time and energy cost. To achieve the goal, it applies stochastic mini-batch dropping, selective layer update, and sign prediction for low-cost backpropagation. Offline on-device training is considered a prerequisite for continual learning. Unlike these studies, we tackle practical on-device CL directly.

9 CONCLUSION

In this work, we investigate the design space of HEM to share insights on enabling cost-effective on-device CL. To

achieve this, we introduce Miro, a system runtime that optimizes HEM for cost-effectiveness under various HW resource constraints. Miro dynamically reconfigures HEM through runtime profiling to adapt to the current learning conditions rather than relying on simple heuristics or past decisions. We evaluate the practicality of Miro mainly using image classification. Our source code will be available to make it possible to reproduce the results.

REFERENCES

- [1] Carousel memory (carm) - official pytorch implementation. <https://github.com/supersob/CarM>.
- [2] Convenient power measurements on the jetson tx2/tegra x2 board. <https://embeddeddl.wordpress.com/2018/04/25/convenient-power-measurements-on-the-jetson-tx2-tegra-x2-board/>.
- [3] Jetson tx2 module. <https://developer.nvidia.com/embedded/jetson-tx2>.
- [4] Jetson xavier nx series. <https://www.nvidia.com/en-us/autonomous-machines/embedded-systems/jetson-xavier-nx>.
- [5] Oem product design guide: Nvidia jetson tx2. <https://usermanual.wiki/Pdf/jetsontx2oemproductdesignguide.2134990230.pdf>.
- [6] Python shared memory. <https://docs.python.org/3/library/multiprocessing.html>.
- [7] Tiny ImageNet visual recognition challenge. <https://tiny-imagenet.herokuapp.com>.
- [8] Urbansound8k dataset. <https://urbansounddataset.weebly.com/urbansound8k.html>.
- [9] J. Bang, H. Kim, Y. Yoo, J.-W. Ha, and J. Choi. Rainbow memory: Continual learning with a memory of diverse samples. In *CVPR*, 2021.
- [10] B. Barshan and K. Altun. Daily and Sports Activities. UCI Machine Learning Repository, 2013. DOI: <https://doi.org/10.24432/C5C59F>.
- [11] R. Bhardwaj, Z. Xia, G. Ananthanarayanan, J. Jiang, N. Karianakis, Y. Shu, K. Hsieh, V. Bahl, and I. Stoica. Ekya: Continuous learning of video analytics models on edge compute servers. In *NSDI*, 2022.
- [12] Z. Borsos, M. Mutny, and A. Krause. Coresets via bilevel optimization for continual learning and streaming. In *NeurIPS*, 2020.
- [13] P. Buzzega, M. Boschini, A. Porrello, D. Abati, and S. CALDERARA. Dark experience for general continual learning: a strong, simple baseline. In *NeurIPS*, 2020.
- [14] F. M. Castro, M. J. Marin-Jimenez, N. Guil, C. Schmid, and K. Alahari. End-to-end incremental learning. In *ECCV*, 2018.
- [15] A. Chaudhry, P. K. Dokania, T. Ajanthan, and P. H. S. Torr. Riemannian walk for incremental learning: Understanding forgetting and intransigence. In *ECCV*, 2018.
- [16] A. Chaudhry, M. Ranzato, M. Rohrbach, and M. Elhoseiny. Efficient lifelong learning with A-GEM. In *ICLR*, 2019.
- [17] A. Chaudhry, M. Rohrbach, M. Elhoseiny, T. Ajanthan, P. K. Dokania, P. H. Torr, and M. Ranzato. On tiny episodic memories in continual learning. *arXiv:1902.10486*, 2019.
- [18] J. Chauhan, Y. D. Kwon, P. Hui, and C. Mascolo. Contauth: Continual learning framework for behavioral-based user authentication. *IMWUT*, 4(4):1–23, 2020.
- [19] T. Chen, B. Xu, C. Zhang, and C. Guestrin. Training deep nets with sublinear memory cost. *arXiv preprint arXiv:1604.06174*, 2016.
- [20] Y. Cong, M. Zhao, J. Li, S. Wang, and L. Carin. GAN memory with no forgetting. In *NeurIPS*, 2020.
- [21] A. Diwan, C.-F. Yeh, W.-N. Hsu, P. Tomasello, E. Choi, D. Harwath, and A. Mohamed. Continual learning for on-device speech recognition using disentangled conformers. *arXiv preprint arXiv:2212.01393*, 2022.
- [22] K. Fall and S. Floyd. Simulation-based comparisons of Tahoe, Reno and Sack TCP. *SIGCOMM Comput. Commun. Rev.*, 26(3):5–21, jul 1996.
- [23] A. Gepperth and B. Hammer. Incremental Learning Algorithms and Applications. In *ESANN*, 2016.
- [24] I. Gim and J. Ko. Memory-efficient dnn training on mobile devices. In *MobiSys*, 2022.
- [25] A. Griewank and A. Walther. Algorithm 799: Revolve: An implementation of checkpointing for the reverse or adjoint mode of computational differentiation. *ACM Trans. Math. Softw.*, 26(1):19–45, mar 2000.
- [26] S. Ha, I. Rhee, and L. Xu. Cubic: A new tcp-friendly high-speed tcp variant. *SIGOPS Oper. Syst. Rev.*, 42(5):64–74, jul 2008.
- [27] T. L. Hayes and C. Kanan. Online continual learning for embedded devices. In *Conference on Lifelong Learning Agents*, 2022.
- [28] K. He, X. Zhang, S. Ren, and J. Sun. Deep residual learning for image recognition. In *CVPR*, pages 770–778. IEEE Computer Society, 2016.
- [29] W. Hu, Z. Lin, B. Liu, C. Tao, Z. Tao, J. Ma, D. Zhao, and R. Yan. Overcoming catastrophic forgetting via model adaptation. In *ICLR*, 2019.
- [30] G. Huang, Y. Sun, Z. Liu, D. Sedra, and K. Q. Weinberger. Deep networks with stochastic depth. In *European Conference on Computer Vision*, 2016.
- [31] Y. Huang, Y. Cheng, A. Bapna, O. Firat, M. X. Chen, D. Chen, H. Lee, J. Ngiam, Q. V. Le, Y. Wu, and Z. Chen. Gpipe: Efficient training of giant neural networks using pipeline parallelism. In *NeurIPS*, 2019.
- [32] M. Khani, G. Ananthanarayanan, K. Hsieh, J. Jiang, R. Netravali, Y. Shu, M. Alizadeh, and V. Bahl. Recl: Responsive resource-efficient continuous learning for video analytics. In *NSDI*, 2023.
- [33] A. Krizhevsky, G. Hinton, et al. Learning multiple layers of features from tiny images. 2009.
- [34] Y. D. Kwon, J. Chauhan, A. Kumar, P. H. HKUST, and C. Mascolo. Exploring system performance of continual learning for mobile and embedded sensing applications. In *IEEE/ACM SEC*, 2021.
- [35] S. Lee, M. Weerakoon, J. Choi, M. Zhang, D. Wang, and M. Jeon. Carm: Hierarchical episodic memory for continual learning. In *DAC*, 2022.
- [36] C. F. S. Leite and Y. Xiao. Resource-efficient continual learning for sensor-based human activity recognition. *ACM Transactions on Embedded Computing Systems*, 21(6):1–25, 2022.
- [37] Y. Liu, Y. Su, A.-A. Liu, B. Schiele, and Q. Sun. Mnemonics training: Multi-class incremental learning without forgetting. In *CVPR*, pages 12245–12254. Computer Vision Foundation / IEEE, 2020.
- [38] D. Lopez-Paz and M. Ranzato. Gradient episodic memory for continual learning. In *NeurIPS*, 2017.
- [39] M. McCloskey and Neal. Catastrophic interference in connectionist networks: The sequential learning problem. In *Psychology of Learning and Motivation*, 1989.
- [40] L. Pellegrini, V. Lomonaco, G. Graffieti, and D. Maltoni. Continual learning at the edge: Real-time training on smartphone devices. *arXiv preprint arXiv:2105.13127*, 2021.
- [41] A. Prabhu, H. A. Al Kader Hammoud, P. K. Dokania, P. H. Torr, S.-N. Lim, B. Ghanem, and A. Bibi. Computationally budgeted continual learning: What does matter? In *Proceedings of the IEEE/CVF Conference on Computer Vision and Pattern Recognition (CVPR)*, pages 3698–3707, June 2023.
- [42] A. Prabhu, P. H. Torr, and P. K. Dokania. GDumb: A simple approach that questions our progress in continual learning. In *ECCV*, 2020.
- [43] S.-A. Rebuffi, A. Kolesnikov, G. Sperl, and C. H. Lampert. iCaRL: Incremental classifier and representation learning. In *CVPR*, 2017.
- [44] D. Rolnick, A. Ahuja, J. Schwarz, T. P. Lillicrap, and G. Wayne. Experience replay for continual learning. 2019.
- [45] O. Russakovsky, J. Deng, H. Su, J. Krause, S. Satheesh, S. Ma, Z. Huang, A. Karpathy, A. Khosla, M. Bernstein, et al. Imagenet large scale visual recognition challenge. *Int J Comput Vis*, 115:211–252, 2015.
- [46] J. Salamon and J. P. Bello. Deep convolutional neural networks and data augmentation for environmental sound classification. *IEEE Signal Processing Letters*, 24:279–283, 2016.
- [47] M. Schiemer, L. Fang, S. Dobson, and J. Ye. Online continual learning for human activity recognition. *Available at SSRN 4357622*.
- [48] A. Seff, A. Beatson, D. Suo, and H. Liu. Continual learning in generative adversarial nets. *arXiv preprint arxiv:1705.08395*, 2017.
- [49] K. Shaheen, M. A. Hanif, O. Hasan, and M. Shafique. Continual learning for real-world autonomous systems: Algorithms, challenges and frameworks. *Journal of Intelligent & Robotic Systems*, 105(1):9, 2022.
- [50] D. Shim, Z. Mai, J. Jeong, S. Sanner, H. Kim, and J. Jang. Online class-incremental continual learning with adversarial shapley value. In *AAAI*, 2021.

- [51] H. Shin, J. K. Lee, J. Kim, and J. Kim. Continual learning with deep generative replay. In *NeurIPS*, 2017.
- [52] G. Sokar, D. C. Mocanu, and M. Pechenizkiy. Spacenet: Make free space for continual learning. *Neurocomputing*, 439:1–11, 2020.
- [53] K. N. Vokinger, S. Feuerriegel, and A. S. Kesselheim. Continual learning in medical devices: Fda’s action plan and beyond. *The Lancet Digital Health*, 3(6):e337–e338, 2021.
- [54] Q. Wang, M. Xu, C. Jin, X. Dong, J. Yuan, X. Jin, G. Huang, Y. Liu, and X. Liu. Melon: Breaking the memory wall for resource-efficient on-device machine learning. In *MobiSys*, 2022.
- [55] Y. Wang, Z. Jiang, X. Chen, P. Xu, Y. Zhao, Y. Lin, and Z. Wang. E2-train: Training state-of-the-art cnns with over 80% energy savings. In *NeurIPS*, 2019.
- [56] Z. Wang, Z. Zhan, Y. Gong, G. Yuan, W. Niu, T. Jian, B. Ren, S. Ioannidis, Y. Wang, and J. Dy. Sparcl: Sparse continual learning on the edge. In *NeurIPS*, 2022.
- [57] C. Wu, L. Herranz, X. Liu, Y. Wang, J. Van de Weijer, and B. Raducanu. Memory Replay GANs: learning to generate images from new categories without forgetting. In *NeurIPS*, 2018.
- [58] Y. Wu, Y. Chen, L. Wang, Y. Ye, Z. Liu, Y. Guo, and Y. Fu. Large scale incremental learning. In *CVPR*, 2019.
- [59] L. Yang, S. Lin, F. Zhang, J. Zhang, and D. Fan. Efficient self-supervised continual learning with progressive task-correlated layer freezing. *ArXiv*, abs/2303.07477, 2023.
- [60] J. You, J.-W. Chung, and M. Chowdhury. Zeus: Understanding and optimizing gpu energy consumption of dnn training. In *NSDI*, 2023.
- [61] Y. Zhao, D. Saxena, and J. Cao. Memory-efficient domain incremental learning for internet of things. In *SenSys*, 2023.